Soft Matter

PAPER

Shear rheology of hydrophobin adsorption layers at oil/water interfaces and data interpretation in terms of a viscoelastic thixotropic model†

Cite this: *Soft Matter*, 2014, **10**, 5777

Gergana M. Radulova,[a] Krassimir D. Danov,[a] Peter A. Kralchevsky,*[a] Jordan T. Petkov‡[b] and Simeon D. Stoyanov[cde]

Here, we investigate the surface shear rheology of class II HFBII hydrophobin layers at the oil/water interface. Experiments in two different dynamic regimes, at a fixed rate of strain and oscillations, have been carried out with a rotational rheometer. The rheological data obtained in both regimes comply with the same viscoelastic thixotropic model, which is used to determine the surface shear elasticity and viscosity, E_{sh} and η_{sh}. Their values for HFBII at oil/water interfaces are somewhat lower than those at the air/water interface. Moreover, E_{sh} and η_{sh} depend on the nature of oil, being smaller for hexadecane in comparison with soybean-oil. It is remarkable that E_{sh} is independent of the rate of strain in the whole investigated range of shear rates. For oil/water interfaces, E_{sh} and η_{sh} determined for HFBII layers are considerably greater than for other proteins, like lysozyme and β-casein. It is confirmed that the hydrophobin forms the most rigid surface layers among all investigated proteins not only for the air/water, but also for the oil/water interface. The wide applicability of the used viscoelastic thixotropic model is confirmed by analyzing data for adsorption layers at oil/water interfaces from lysozyme and β-casein – both native and cross-linked by enzyme, as well as for films from asphaltene. This model turns out to be a versatile tool for determining the surface shear elasticity and viscosity, E_{sh} and η_{sh}, from experimental data for the surface storage and loss moduli, G' and G''.

Received 25th April 2014
Accepted 3rd June 2014

DOI: 10.1039/c4sm00901k

www.rsc.org/softmatter

1. Introduction

Hydrophobins are stable, relatively small cysteine-rich proteins composed of 70–100 amino acids. The foams from aerated solutions of the class II hydrophobin HFBII exhibit exceptional stability across a wide range of pH.[1,2] Biotechnically produced hydrophobins can stabilize gel-like emulsions with an oil mass fraction above 65% and Pickering emulsions with hydrophobin-decorated clay nanoparticles.[3–8] Hydrophobins are sticky molecules[9,10] that have found applications also for immobilization of functional molecules at surfaces[11] and as coating agents for surface modification.[12,13]

Surface rheological properties have a significant impact on the dynamics and stability of foams and emulsions.[14–17] Dense adsorption layers that exhibit higher surface elasticity and viscosity can suppress the Ostwald ripening and the coalescence of bubbles or drops.[18] At an air/water interface, HFBII forms films of high mechanical strength with markedly greater surface dilatational and shear moduli than those of other proteins.[2,19–23] The HFBII adsorption layers undergo a transition from the two-dimensional fluid to the elastic membrane much faster (after several minutes)[19] than the common milk and egg proteins, which acquire shear elasticity after 8 to 24 hours.[24] The addition of HFBII to solutions of milk proteins enhances the stability of foams produced from these solutions.[25,26]

The properties of hydrophobin adsorption layers have been studied mostly at the air/water interface. There are only a few studies on hydrophobin layers at oil/water interfaces. The interfacial tension of HFBII at hexane–water relaxes to about 30 mN m^{-1} after several minutes.[27] Using molecular dynamics simulations with a chemically detailed coarse-grained potential, the behavior of hydrophobins at the octane–water interface is studied.[28] The calculations of the interfacial adsorption energy indicate that the hydrophobin adsorption is essentially irreversible.[28]

The surface shear rheology of protein adsorption layers at oil/water interfaces is less studied than that at the air/water

[a]*Department of Chemical Engineering, Faculty of Chemistry & Pharmacy, Sofia University, 1164 Sofia, Bulgaria. E-mail: pk@lcpe.uni-sofia.bg; Tel: +359 2 8161262*
[b]*Unilever Research & Development, Port Sunlight, Wirral, Merseyside CH63 3JW, UK*
[c]*Unilever Research & Development, 3133AT Vlaardingen, The Netherlands*
[d]*Laboratory of Physical Chemistry & Colloid Science, Wageningen University, 6703 HB Wageningen, The Netherlands*
[e]*Department of Mechanical Engineering, University College London, Torrington Place, London, WC1E 7JE, UK*

† Electronic supplementary information (ESI) available: Appendix A: applications of the VT model: (1) effect of enzyme on the rigidity of β-casein layers; (2) rheology of asphaltene films at toluene–heptane/brine interfaces and interfacial-tension relaxation. Appendix B: solidification of a HFBII layer at the o/w interface. See DOI: 10.1039/c4sm00901k

‡ Present address: KL-Kepong Oleomas SDN BHD, Menara KLK, Jalan PJU 7/6, Mutiara Damansara, 47810 Petaling Jaya, Selangor Dalur Ehsan, Malaysia.

boundary; for review, see ref. 29 and 30. It was found that in the presence of mono- and diglycerides, the viscoelasticity of sodium caseinate adsorption layers at corn-oil/water interfaces significantly increases as indicated by the creep-compliance-time behavior.[31] A rotational rheometer with a biconical disc was used for studies of the interactions between tristearin crystals and lysozyme at the tetradecane–water interface.[32] An interfacial stress rheometer based on a thin magnetized rod was applied to measure the shear storage, G', and loss, G'', moduli of lysozyme and β-casein adsorption layers at hexadecane/water interfaces.[33,34] The addition of transglutaminase enzyme was found to induce cross-linking in β-casein adsorption layers at the tetradecane/water interface and to increase the shear storage and loss moduli.[35] The adsorption of bovine serum albumin, lysozyme and insulin to oil/water interfaces has been characterized by interfacial shear stress measurements using a sensitive rheometer with a Du-Noüy-ring.[36] The effects of added sodium dodecyl sulphate[37] and heat-induced fibers of β-lactoglobulin[38] on the shear rheology of β-lactoglobulin adsorption layers at oil/water interfaces have also been examined. A rotational rheometer with a biconical disc was used to measure the surface rheological properties of liquid–liquid interfaces stabilized by protein fibrillar aggregates and protein–polysaccharide complexes.[39] The shear rheology of oil/water interfaces has been used to characterize also some specific systems like recombinant spider-silk proteins[40] and asphaltenes.[41]

The determination of the surface shear elasticity and viscosity, E_{sh} and η_{sh}, from the measured shear storage and loss moduli, G' and G'', is possible in the frames of a given rheological model. Different rheological models lead to different relations between E_{sh} and η_{sh} with the experimentally determined G' and G''. It was established[20–22] that the rheological behavior of β-lactoglobulin, β-casein, HFBII, and mixed layers of HFBII with β-casein, β-lactoglobulin, ovalbumin and Tween 20 at the air/water interface obeys a viscoelastic thixotropic (VT) model. The determined shear elasticity and viscosity represent universal functions of the rate of strain irrespective of the used different dynamic regimes: fixed rate of strain and oscillations.

Here, we report results on shear rheology of adsorption layers from a class II hydrophobin, *viz*. HFBII, on hexadecane/water and soybean-oil/water interfaces. To the best of our knowledge, this is the first study on surface shear rheology of hydrophobin layers at the *oil/water* interface. The rotational rheometer was used in two different dynamic regimes: fixed rate of strain and oscillations. Further, the VT model is applied to interpret the data obtained in both regimes and to determine E_{sh} and η_{sh} as functions of the shear rate. The results for three different nonpolar fluid phases, air, mineral oil and vegetable oil, are compared and discussed. The applicability of the VT model is also verified against literature data for G' and G'' for adsorption layers from lysozyme,[34] β-casein[34,35] and asphaltenes[41] at oil/water interfaces.

2 Materials and methods

2.1 Materials

In our measurements, the oil phase comprised of *n*-hexadecane (C16) or soybean oil (SBO). The used hexadecane was a product of Merck with 99% purity. It was additionally purified by passing it twice through a column filled with silica gel (Merck, Germany) and activated magnesium silicate (Florisil, Sigma-Aldrich, Germany). The interfacial tension of the purified hexadecane against pure water was 54.0 ± 0.5 mN m^{-1}, which is close to the literature data.[42] The viscosity of hexadecane is 3.06 mPa s at 25 °C.[43]

The SBO was a food grade commercial product from a local producer, which was purified by passing through a column filled with the adsorbent bentonite (Teokom, Bulgaria) and activated magnesium silicate. Up to three consecutive passages were applied to obtain oil that is free of substances decreasing its interfacial tension against water with more than 0.2 mN m^{-1} for 30 minutes. The value of the interfacial tension of the *purified* SBO was 30.5 ± 0.5 mN m^{-1}, which is close to the literature value of 31 mN m^{-1}.[44] The viscosity of SBO is 54.3 mPa s at 25 °C,[45] *i.e.* the SBO is considerably more viscous than hexadecane.

For the preparation of all solutions, deionized water of specific resistivity 18.2 MΩ cm (Elix purification system, Millipore) was used. All experiments were performed at a temperature of 25 °C.

In our experiments, we used hydrophobin HFBII produced *via* fermentation using *Trichoderma reesei*.[9] The HFBII sample was provided as a gift by Unilever R&D. The molecular weight of HFBII is 7.2 kDa. It is composed of 70 amino acids with 4 disulfide bonds. In all described experiments the concentration of HFBII in the aqueous phase was 0.005 wt%. Just before each measurement, the solutions were sonicated in an ultrasound bath for 5 min to disperse the formed protein aggregates.

At both air/water and oil/water interfaces, the interfacial tension, σ, of HFBII solutions first decreases with the rise of hydrophobin concentration, and then it levels off at higher concentrations; see *e.g.* ref. 46. At the working concentration of 0.005 wt% HFBII in the aqueous phase, for the SBO/water interface σ decreases from 30.5 to 18.4 mN m^{-1} within 10 seconds, and then it remains constant with indications for surface "solidification", *i.e.* for the formation of an elastic (rather than fluid) interfacial film; see Fig. B1 in Appendix B.† The surface solidification means that a dense HFBII adsorption layer is formed at the oil/water interface. The present study is dedicated to the investigation of the surface shear elasticity and viscosity, E_{sh} and η_{sh}, of such *dense* layers. At lower HFBII concentrations, non-densely packed HFBII adsorption layers of lower E_{sh} and η_{sh} are expected to form, as detected by Cox *et al.*[46] and Aumaitre *et al.*[47] for the air/water interface. For oil/water interfaces, this effect could be a subject of a subsequent study.

2.2 Methods

Surface shear rheometry. Interfacial shear rheology measurements were performed using a rotational rheometer Bohlin Gemini, Malvern UK, equipped with a biconical disc (Fig. 1).[48–50] The bicone was first positioned at the air/water interface. Next, the oil phase was gently poured on top of the solution until it formed a layer of thickness 2–3 mm. We waited 5 min before the start of the rheological measurements. This time is large enough for a complete formation of viscoelastic

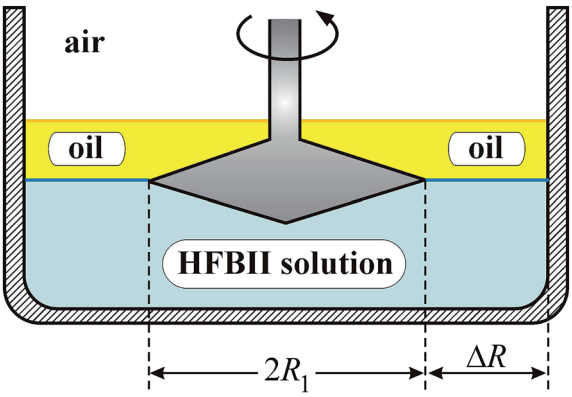

Fig. 1 Sketch of the used rotational rheometer with a biconical disc. The dimensions are $R_1 = 2.81$ cm and $\Delta R = R_2 - R_1 = 0.19$ cm. The thickness of the oil layer is 2–3 mm.

HFBII adsorption layers.[20–22] To check the reproducibility of the results, every experiment was repeated at least three times, each time with new portions of HFBII solution and oil.

The primary data given by the apparatus are the rotation angle, θ, and the torque, τ, as functions of time t. The greatest rotation angle used in our experiments was 21 mrad, so that the shear strain, $\gamma \equiv \tan\theta$, can be approximately written as $\gamma \approx \theta$ with a relative error that is smaller than 1.5×10^{-4}. For that reason, we will use γ for both shear strain (measured in %) and rotation angle (measured in radians); 1 mrad = 0.1%. The outer radius of the bicone is $R_1 = 2.81$ cm; the inner radius of the wall of the cylindrical cell is $R_2 = 3.00$ cm, and the distance between them is $\Delta R = R_2 - R_1 = 0.19$ cm. The latter represents the width of the ring-shaped adsorption layer that is subjected to shear deformation (Fig. 1). The surface shear stress, τ_{sh}, is calculated from the measured torque τ using the formula $\tau_{sh} = g_f\tau$, where $g_f = (R_1^{-2} - R_2^{-2})/4\pi = 12.36$ rad m^{-2} is the geometrical factor of the used configuration.[20–22]

Oscillatory regime. In this regime, the rotation angle oscillates with fixed amplitude γ_a and frequency ν. The corresponding periodic variations in the torque are registered. Experiments have been carried out at amplitudes γ_a = 1.75, 5.23, 10.5, and 21 mrad and frequencies $\nu = 0.01$, 0.02, 0.05, 0.1, 0.2, 0.5, 1, and 2 Hz. Higher frequencies and amplitudes were not used because analogous rheological experiments at air/water interfaces showed that the HFBII layers break at $\nu > 2$ Hz and/or $\gamma_a \geq 21$ mrad.[21]

In the oscillatory regime, the variations of the shear strain, γ, are sinusoidal:

$$\gamma = \gamma_a \sin(\omega t), \quad (1)$$

where: $\gamma_a > 0$ is the amplitude; $\omega = 2\pi\nu$ is the angular frequency. The fits of the experimental data for $\gamma(t)$ with eqn (1) (Fig. 2a and b) showed that the oscillations of γ are also sinusoidal. In general, the registered shear stress τ_{sh} can be expressed in the form:

$$\frac{\tau_{sh}}{\gamma_a} = G' \sin(\omega t) + G'' \cos(\omega t), \quad (2)$$

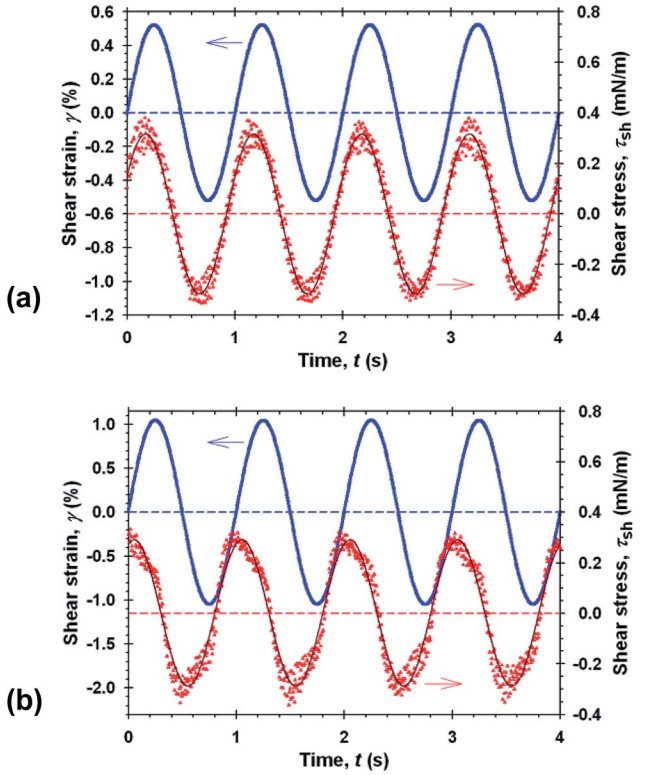

Fig. 2 Illustrative dependences of the applied shear strain, γ, and the measured shear stress, τ_{sh}, on time t for adsorption layers from 0.005 wt% aqueous HFBII solution at the oil/water interface at frequency $\nu = 1$ Hz: (a) The oil is hexadecane; the strain amplitude is $\gamma_a = 0.522\%$. (b) The oil is SBO; $\gamma_a = 1.05\%$. The solid lines for τ_{sh} are the best fits with eqn (2).

where G' and G'' are the storage and loss moduli, respectively. For a *true linear* response, G' and G'' do not depend on ω and γ_a, whereas for a *quasi-linear* response (observed in our experiments) they depend on the rate of strain amplitude,[21,22] *i.e.* on the product $\gamma_a\omega$.

Small systematic deviations from the linear regime are visible in Fig. 2b at the greater strain amplitude $\gamma_a = 1.05\%$. In such a case, the Fourier expansion of $\tau_{sh}(t)$ contains also the third, fifth, *etc.* odd harmonics.[21] We checked that under the used experimental conditions ($\nu \leq 2$ Hz and $\gamma_a < 2.1\%$) the contribution of the higher harmonics to the calculated G' and G'' is negligible.

Thus, in each separate oscillatory experiment we worked at *fixed* frequency and strain amplitude, ω and γ_a. Two alternative automatic oscillatory regimes can be realized with the rotational rheometers: (i) *frequency sweep*: the frequency varies at fixed strain amplitude and (ii) *strain sweep* the strain amplitude varies at a fixed frequency. We did not use the sweep regimes, because the respective measurements usually take longer time and the protein adsorption layers could be affected by aging effects.

Fixed-rate-of-strain regime. In this regime, called also "angle ramp",[20] the rotation angle γ increases with a *constant rate*, $\dot{\gamma}$, during a given period of time (200 and 400 s in our experiments). During the whole experiment, γ and τ_{sh} were recorded

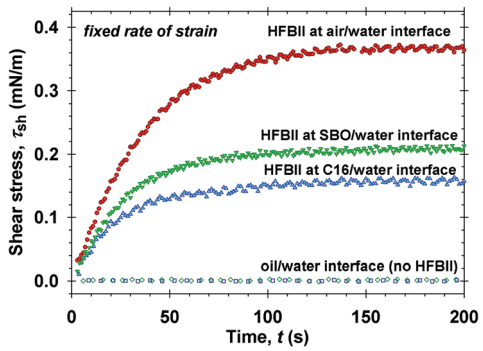

Fig. 3 Illustrative plot of the shear stress, τ_{sh}, *vs.* time, t: data obtained in fixed-rate-of-strain regime at fixed $\dot{\gamma} = 35$ μrad s^{-1} for air/water and oil/water interfaces with and without HFBII in the aqueous phase, as denoted in the figure. For the three upper curves, the HFBII concentration is 0.005 wt%.

as functions of time, t. Fig. 3 shows illustrative data for the dependence of the stress τ_{sh} on t at $\dot{\gamma} = 35$ μrad s^{-1}. The apparatus produces a perfect linear dependence of the strain, $\gamma = \dot{\gamma}t$. The final value of the strain is $\gamma_b = 0.7\%$, corresponding to a period of 200 s.

Low shear rates, $8.75 \leq \dot{\gamma} \leq 280$ μrad s^{-1}, have been used in our experiments. Under such conditions, in the absence of HFBII (pure aqueous phase) we measured $\tau_{sh} = 0$ in the frames of the experimental accuracy; see the lowest curve in Fig. 3. In other words, at such low shear rates the bulk friction in the adjacent oil and water phases does not contribute to the registered signal. This is fulfilled for both hexadecane and the more viscous SBO. Hence, the whole signal registered in our experiments is due to the protein adsorption layer.

As seen in Fig. 3, the shear stress τ_{sh} registered for HFBII adsorption layers at the oil/water interfaces is about 2 times lower than at the air/water interface. Despite that, τ_{sh} can be registered with a good precision for the investigated oil/water interfaces. We could hypothesize that these lower τ_{sh} values might be due to the penetration of oil molecules between the hydrophobin molecules in the adsorption layer. These oil molecules could act as a lubricant that reduces the rigidity of the HFBII layer. The experimental data are presented in Section 3 and interpreted in Section 4.

3. Experimental results and discussion

3.1 Fixed-rate-of-strain regime

Fig. 4 shows experimental results for the shear stress, τ_{sh}, *versus* time at six different values of the angular velocity (shear rate), $\dot{\gamma}$, varying from 8.75 μrad s^{-1} to 280 μrad s^{-1}. At greater $\dot{\gamma}$, the values of the measured shear stress τ_{sh} are also greater. At higher angular velocities, the experimental curves are slightly undulated. This is due to the action of a mechano–electronic feedback built in the apparatus, which keeps $\dot{\gamma}$ constant.

In Fig. 3 and 4, τ_{sh} is markedly lower for the hexadecane/water interface in comparison with the SBO/water interface

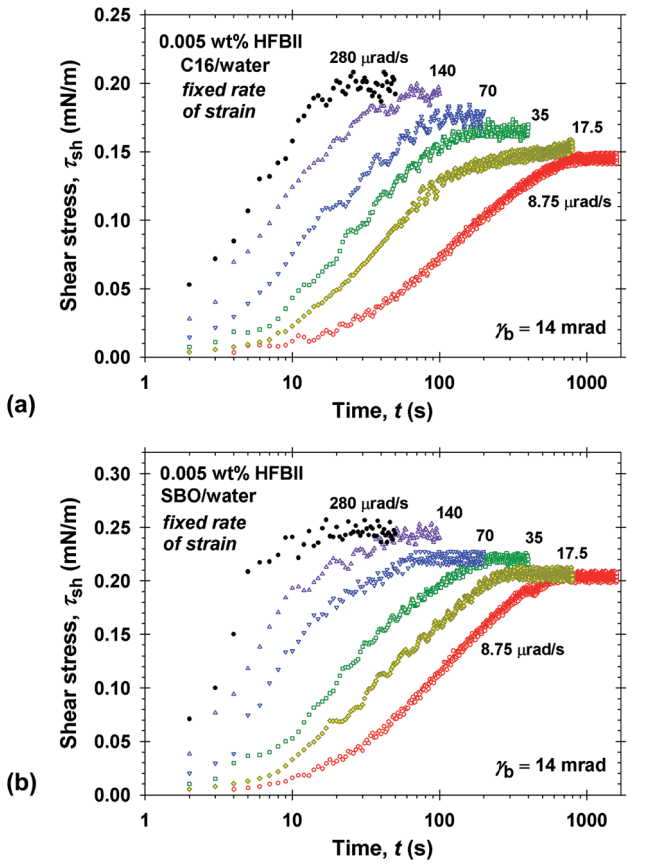

Fig. 4 Plots of the shear stress, τ_{sh}, *vs.* time, t, at six different fixed angular velocities $\dot{\gamma}$ denoted in the figure. The data are for adsorption layers at the interface between 0.005 wt % aqueous solution of HFBII and (a) hexadecane and (b) soybean oil. The rotation angle increases up to a maximal value $\gamma_b = 14$ mrad.

(compare Fig. 4a and b). This could be explained with the smaller size of the hexadecane molecules as compared to the triglycerides in the SBO. The smaller oil molecules could more easily penetrate into the hydrophobin adsorption layer and reduce its rigidity.

The shapes of the experimental curves in Fig. 3 and 4 are similar to those for HFBII adsorption layers at the air/water interface.[20–22] Such shape of the stress-*vs.*-strain dependence is predicted by the Maxwell model, where the total strain γ is equal to the sum of the deformations of the elastic and viscous elements; see the inset in Fig. 5. In terms of rates-of-strain, this reads:

$$\frac{1}{E_{sh}}\frac{d\tau_{sh}}{dt} + \frac{\tau_{sh}}{\eta_{sh}} = \frac{d\gamma}{dt}, \quad (3)$$

where E_{sh} and η_{sh} are the shear elasticity and viscosity, respectively. The integration of eqn (3) at constant E_{sh} and η_{sh} yields:

$$\tau_{sh} = \eta_{sh}\dot{\gamma}\left[1 - \exp\left(-\frac{E_{sh}}{\eta_{sh}}t\right)\right]. \quad (4)$$

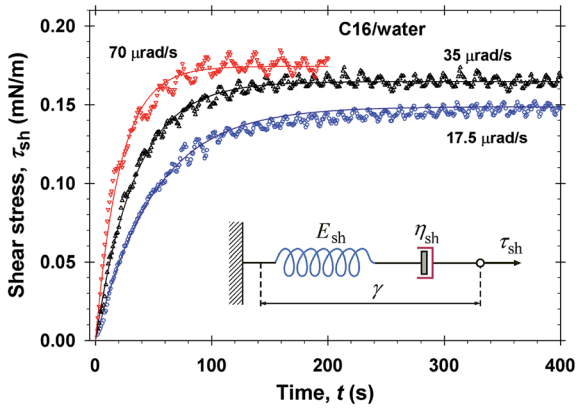

Fig. 5 Typical dependencies of the shear stress, τ_{sh}, on time, t, obtained in the fixed-rate-of-strain regime at different fixed angular velocities, $\dot{\gamma}$; the oil phase is hexadecane (C16). The solid lines are fits by the Maxwell model, eqn (4). The inset shows a sketch of the Maxwell model of a viscoelastic body: consecutively connected elastic element (spring) of modulus E_{sh} and viscous element (dash-pot) characterized by viscosity coefficient η_{sh}.

Fig. 5 shows fits of experimental curves with eqn (4). From each fit, E_{sh} and η_{sh} are determined as adjustable parameters. The results indicate that the viscosity η_{sh} is calculated with a good precision, whereas the values of the shear elasticity are scattered around the values $E_{sh} = 108$ mN m^{-1} for C16 and $E_{sh} = 149$ mN m^{-1} for SBO, which are obtained in the oscillatory regime; see Section 3.2. For this reason, we fitted all experimental curves obtained in the fixed-rate-of-strain regime by varying only one adjustable parameter, η_{sh}, at fixed E_{sh} values equal to those determined in the oscillatory regime. The obtained values of η_{sh} are plotted in Fig. 6 *versus* the shear rate.

As seen in Fig. 5, even a single adjustable parameter, η_{sh}, provides a very good agreement between the calculated and experimental curves – the regression coefficients are greater than 0.996. The relative scattering of the experimental data for the oil/water interface is greater than that for the air/water interface[20–22] at the same shear rates. This is because for the oil/water interface the oscillations due to the automatic feedback are superimposed on lower τ_{sh} values.

Fig. 6 compares the results for η_{sh} *vs.* $\dot{\gamma}$ obtained for C16/water and SBO/water interfaces with those from ref. 21 for the air/water interface. One sees that η_{sh} is the highest for the air/water interface and the lowest for the C16/water interface. The values of the shear elasticity vary in the same order: $E_{sh} = 160$, 149 and 108 mN m^{-1} for the air/water, SBO/water and C16/water interfaces, respectively. As discussed above, this should be expected because the cohesion between the adsorbed HFBII molecules is the strongest at the air/water interface, whereas C16 molecules (smaller than the triglycerides in SBO) can penetrate more easily between the hydrophobin globules and reduce the cohesion between them.

The variation of viscosity η_{sh} with the shear rate $\dot{\gamma}$ (Fig. 6) is not in conflict with the use of the Maxwell model to fit the data (Fig. 5). Indeed, in the fixed-rate-of-strain regime $\dot{\gamma} = $ const. for each run, so that $\eta_{sh}(\dot{\gamma}) = $ const. for each experimental curve, like those in Fig. 3–5.

3.2 Oscillatory regime

Fig. 7 shows the determined values of the storage and loss moduli, G' and G'', as functions of the rate-of-strain amplitude, $\gamma_a\omega$. Each

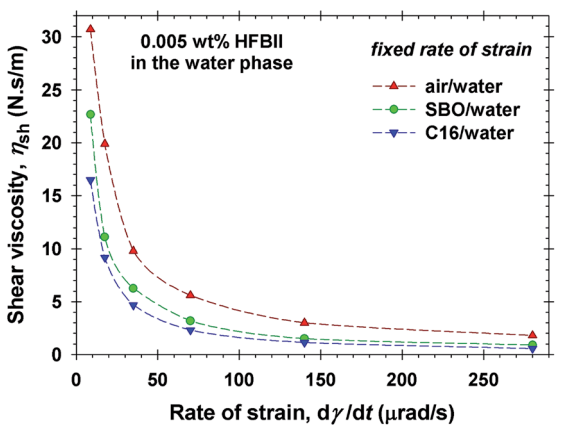

Fig. 6 Plots of the shear viscosity, η_{sh}, *vs.* the rate of strain, $\dot{\gamma}$, for HFBII adsorption layers at the air/water, SBO/water and hexadecane/water interfaces obtained in the fixed-rate-of-strain regime. The lines are a guide to the eye.

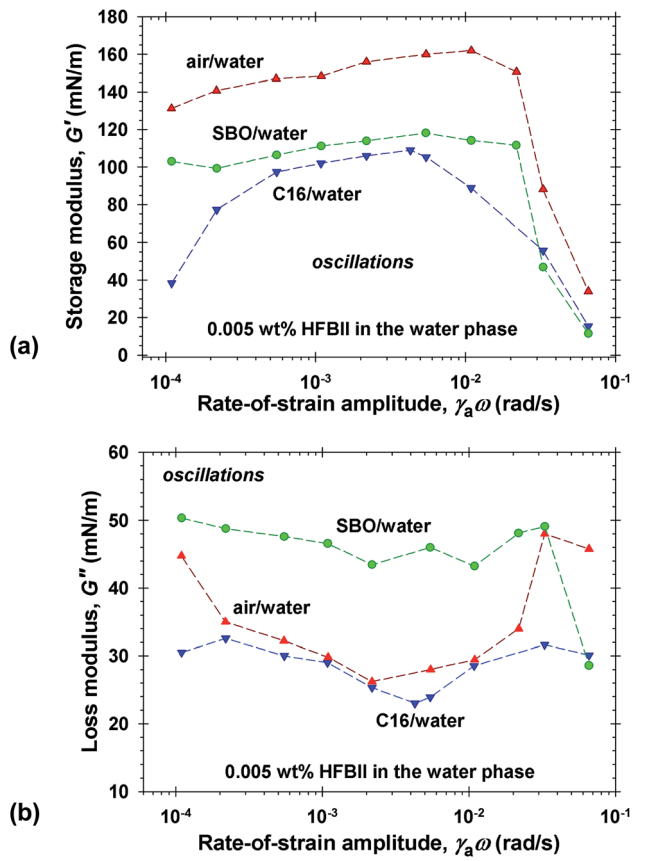

Fig. 7 Plots of experimental data for the surface shear moduli *vs.* the rate-of-strain amplitude, $\gamma_a\omega$, for HFBII adsorption layers at air/water, SBO/water interfaces and C16/water interfaces. (a) Storage modulus G'. (b) Loss modulus G''. The lines are a guide to the eye.

experimental point is the average from six measurements, corresponding to 3 runs with different portions of the working solution with 2 measurements during each run. The duration of the run with a given solution is inversely proportional to the frequency of oscillations. Fig. 7 summarizes data from experiments (i) at fixed amplitude $\gamma_a = 1.75$ mrad and 8 different frequencies between 0.01 to 2 Hz and (ii) at fixed frequency $\nu = 1$ Hz and two different amplitude: $\gamma_a = 5.23$ and 10.5 mrad. In this way, the rate-of-strain amplitude, $\gamma_a\omega$, covers the range from 10^{-4} to 7×10^{-2} rad s^{-1} by varying both the amplitude and frequency.

The data for the storage modulus G' in Fig. 7a follow the same tendency as those in Fig. 3 for τ_{sh} (fixed rate of strain), *viz.* G' is the greatest for HFBII layers at the air/water interface and the lowest for such layers at the C16/water interface. The highest loss modulus G'' is measured for HFBII layers at the SBO/water interface (Fig. 7b).

The moduli G' and G'' are phenomenological parameters defined by eqn (2). The interface can be characterized by shear elasticity and viscosity, E_{sh} and η_{sh}, only in the frames of a given model. As mentioned above, the relations of E_{sh} and η_{sh} with G' and G'' are different for different rheological models.[21] Our data from the experiments in the fixed-rate-of-strain regime (Fig. 5) unequivocally show that the investigated protein layers comply with a model of Maxwell type, *viz.* the VT model, which is briefly presented in the next section.

4. Rheological model

The experimental data obtained in a fixed rate of the strain regime indicate that for each fixed shear rate, $\dot{\gamma}$, the time dependence of the stress τ_{sh} obeys the Maxwell model (Fig. 5). Thus, from the fit of each $\tau_{sh}(t)$ curve with eqn (4) one determines the shear elasticity and viscosity as functions of $\dot{\gamma}$:

$$E_{sh} = E_{sh}(|\dot{\gamma}|),\ \eta_{sh} = \eta_{sh}(|\dot{\gamma}|). \tag{5}$$

In general, the elasticity and viscosity are functions of the absolute value $|\dot{\gamma}|$, because they do not depend on whether the rotation is clockwise or anticlockwise.[21,51]

Eqn (3) with variable E_{sh} and η_{sh} represents the basic equation of the *viscoelastic thixotropic* (VT) model[21] with a single Maxwell element. Acierno *et al.*[52,53] have considered more general models based on a series of Maxwell elements; see also section 8.3 in ref. 54. It is worth noting that numerous experiments with interfacial layers in a Langmuir trough indicate that their viscoelastic behavior complies with the Maxwell model, or its modified versions.[55–59] Our first task here is to check whether the data for HFBII layers at the *oil/water* interface also obey the VT model.

For this goal, let us consider the characteristic frequency, ν_{ch}, defined by the relationship:

$$\nu_{ch}(\gamma) \equiv \frac{E_{sh}(|\dot{\gamma}|)}{\eta_{sh}(|\dot{\gamma}|)}. \tag{6}$$

In the VT model, ν_{ch} is a power function of $|\dot{\gamma}|$:

$$\nu_{ch}(|\dot{\gamma}|) = Q|\dot{\gamma}|^m. \tag{7}$$

For the data obtained in the fixed-rate-of-strain regime, the fulfillment of eqn (7) can be directly verified (see below). For the data obtained in the *oscillatory* regime, the fulfillment of eqn (7) can be verified in terms of the mean characteristic frequency:[21]

$$\langle\nu_{ch}\rangle \equiv \frac{G''}{G'}\omega = \frac{2}{\pi}\int_0^{\pi} \nu_{ch}(\xi)\sin^2\xi\,d\xi, \tag{8}$$

where $\xi \equiv \omega t$ is an integration variable and it is taken into account that $\dot{\gamma} = \gamma_a\omega\cos\xi$. Substituting eqn (7) in eqn (8) and integrating, we obtain:[21]

$$\langle\nu_{ch}\rangle = Q\langle\dot{\gamma}\rangle^m. \tag{9}$$

$$\langle\dot{\gamma}\rangle \equiv \mu\gamma_a\omega\ ,\quad \mu \equiv \left[\frac{\Gamma(m/2+0.5)}{\pi^{1/2}\Gamma(m/2+2)}\right]^{1/m}. \tag{10}$$

Eqn (9) is the averaged form of eqn (7) for the oscillatory regime; $\Gamma(x)$ is the gamma function and μ is a constant.

If ν_{ch} was a constant, independent of time (as it is in the fixed-rate-of-strain regime), then eqn (8) would yield $\langle\nu_{ch}\rangle = \nu_{ch}$, as it should be expected. In the oscillatory regime, G' and G'' are directly obtained from the experimental data, so that the mean characteristic frequency, $\langle\nu_{ch}\rangle = G''\omega/G'$, can be also determined from the data. Eqn (7) and (9) imply that if we plot the data from the fixed-rate-of-strain regime as ν_{ch} *vs.* $\dot{\gamma}$, and the data from the oscillatory regime as $\langle\nu_{ch}\rangle$ *vs.* $\langle\dot{\gamma}\rangle$, in double-log scale both sets of data should comply with the same straight line with slope m and intercept Q. The plots in Fig. 8 indicate that this indeed is fulfilled for HFBII adsorption layers at the C16/water and SBO/water interface. The long-dashed line in Fig. 8 represents the best fit of analogous data for HFBII layers at the air/water interface.[21] These results mean that the rheological behavior of HFBII layers at both the oil/water and air/water interface obey the VT model, which is based on eqn (3) and (7).

For each interface, the parameters m and Q are determined from the slope and the intercept of the straight lines in Fig. 8 in accordance with eqn (7) and (9); μ is calculated from the second formula in eqn (10). The obtained values are given in Table 1,

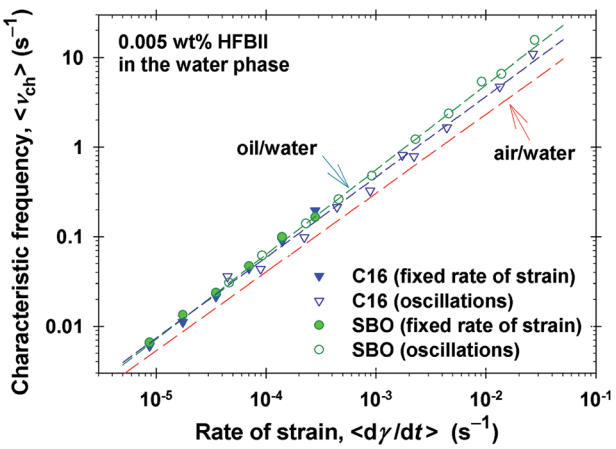

Fig. 8 Plots of the characteristic frequency *vs.* the rate of strain for HFBII adsorption layers at the C16/water, SBO/water and air/water interface, as denoted in the figure. For the fixed-rate-of-strain regime, the plot is ν_{ch} *vs.* $\dot{\gamma}$. For the oscillatory regime, the plot is $\langle\nu_{ch}\rangle$ *vs.* $\langle\dot{\gamma}\rangle$.

Table 1 Rheological parameters determined from the fits of experimental data

Interfaces	m	Q (s^{m-1})	μ	E_{sh} (mN m^{-1})	K (N s^{1-m} m^{-1})
Air/water	0.88	134	0.413	160[a]	1.19×10^{-3a}
C16–water	0.90	233	0.415	108	4.63×10^{-4}
SBO–water	0.95	389	0.419	149	3.83×10^{-4}

[a] Mean values determined in the fixed-rate-of-strain regime.[20]

where comparison data for the air/water interface[20,21] are also shown.

Having determined m, we can further find the mean surface shear elasticity and viscosity, $\langle E_{sh}\rangle$ and $\langle \eta_{sh}\rangle$ from the data for G' and G'' using the respective formulae of the VT model:[21]

$$\langle E_{sh}\rangle = \frac{G'^2 + (m+1)G''^2}{G'}, \quad (11)$$

$$\langle \eta_{sh}\rangle = \frac{G'^2 + (m+1)G''^2}{G''\omega}. \quad (12)$$

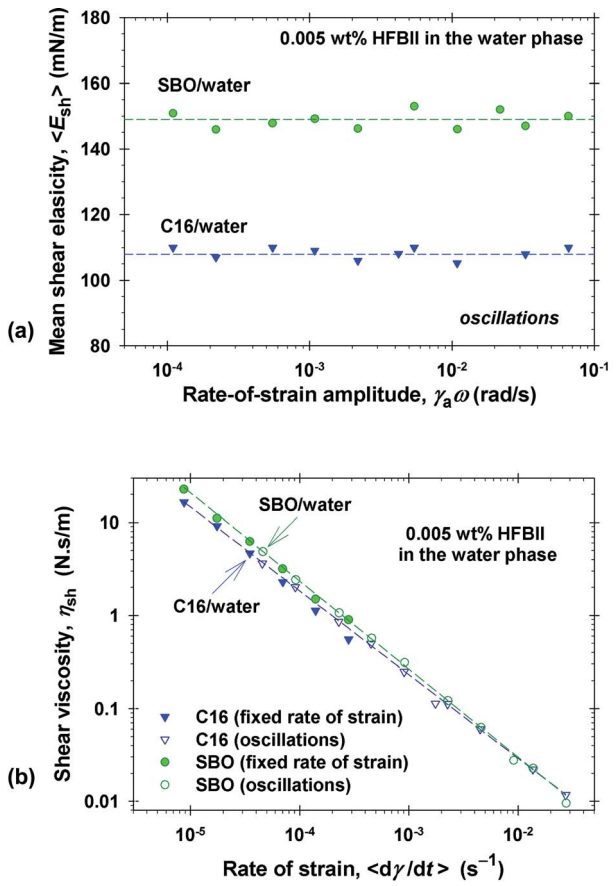

Fig. 9 (a) Plot of the mean shear elasticity $\langle E_{sh}\rangle$ *vs.* the rate-of-strain amplitude $\gamma_a\omega$, calculated from the experimental G' and G'' using eqn (11). (b) Plot of the shear viscosity *vs.* the rate of strain. For the fixed-rate-of-strain regime, the plot is η_{sh} *vs.* $\dot{\gamma}$. For the oscillatory regime, the plot is $\langle \eta_{sh}\rangle$ *vs.* $\langle \dot{\gamma}\rangle$. The lines represent the best fits with the parameters from Table 1.

For $m = 0$ eqn (11) and (12) reduce to known relationships of the conventional Maxwell model.[21] In Fig. 9, the values of $\langle E_{sh}\rangle$ and $\langle \eta_{sh}\rangle$ calculated from the data for G' and G'' in Fig. 7 are shown. It turns out that the *shear elasticity* $\langle E_{sh}\rangle$ is constant, *i.e.* independent of the rate-of-strain amplitude, $\gamma_a\omega$, in the whole range of amplitudes and frequencies investigated (Fig. 9a). This result is remarkable in view of the rather irregular shape of the experimental curves for G' and G'' in Fig. 7a and b. The mean values of E_{sh} are given in Table 1 for the three investigated interfaces. For all of them, the shear elasticity of the HFBII adsorption layers is high, $E_{sh} > 100$ mN m^{-1}. The smallest and the greatest elasticities are determined for the C16/water and air/water interfaces, respectively.

To compare the data for the *shear viscosity* obtained in the two kinetic regimes, in Fig. 9b we have plotted the data from the fixed-rate-of-strain regime (Fig. 6) as η_{sh} *vs.* $\dot{\gamma}$ and for the oscillatory regime – as $\langle \nu_{ch}\rangle$ *vs.* $\langle \dot{\gamma}\rangle$. The plot shows an excellent agreement between the values of η_{sh} obtained in these two different regimes. The values of η_{sh} for the C16/water interface are only slightly smaller than for the SBO/water interface. The linear dependence on the double-log scale (Fig. 9b) follows from eqn (6) and (7):

$$\eta_{ch} = \frac{E_{sh}}{\nu_{sh}} = \frac{E_{sh}}{Q|\dot{\gamma}|^m}, \quad (13)$$

where E_{sh} is constant (Fig. 9a). Eqn (13) indicates decrease of surface viscosity with the rise of the shear rate, $\dot{\gamma}$, *i.e.* shear thinning.

In the conventional Ostwald–de Waele model for viscous bodies ($E_{sh} \equiv 0$),[60] the shear thinning is described by the expression:

$$\tau_{sh} = K\dot{\gamma}^n = \eta_{sh}\dot{\gamma} \quad \Rightarrow \quad \eta_{sh} = K\dot{\gamma}^{n-1}, \quad (14)$$

where the coefficient K is termed consistency, and n is the flow behavior index. The comparison of eqn (13) and (14) shows that $n = 1 - m$, and $K = E_{sh}/Q$. The values of K calculated from the latter expression are also shown in Table 1. Note that the use of eqn (14) and K to characterize the viscosity η_{sh} is meaningful only if E_{sh} is constant [otherwise $K = K(\dot{\gamma})$].

In general, E_{sh} can depend on $\dot{\gamma}$ in the frame of the VT model; see eqn (5). The fact that E_{sh} is constant for HFBII layers at C16/water and SBO/water interfaces in a wide range of shear rates (Fig. 9a) is a remarkable property of these interfacial layers. For HFBII adsorption layers at the air/water interface, E_{sh} is constant only at the lower $\dot{\gamma}$ values.[21] For the mixed adsorption layers of HFBII with β-casein, β-lactoglobulin, ovalbumin and Tween 20 at the *air/water* interface, the plot of E_{sh} *vs.* $\dot{\gamma}$ represents a non-monotonic dependence with a maximum.[21,22]

5. Comparison with data for lysozyme and β-casein

Here, our goal is to verify whether other viscoelastic layers at the oil/water interface also obey the VT model, *i.e.* whether this model can be used as a universal tool to determine the surface

shear elasticity and viscosity, $\langle E_{sh}\rangle$ and $\langle \eta_{sh}\rangle$, from the storage and loss moduli, G' and G''. A criterion for the applicability of the VT model to a given system is whether the characteristic frequency $\langle \nu_{ch}\rangle = G''\omega/G'$ exhibits power law behavior as a function of the strain amplitude $\gamma_a\omega$; see Fig. 8 and eqn (9) and (10). This criterion is applied to analyze sets of published rheological data for lysozyme and β-casein[34] (in this section), as well as for β-casein layers cross-linked by the enzyme transglutaminase,[35] and for asphaltene films at toluene–heptane/brine interfaces[41] (see Appendix A†). The values of $\langle E_{sh}\rangle$ and $\langle \eta_{sh}\rangle$ determined for these adsorption layers are compared with the respective values for HFBII.

In ref. 34, the shear moduli, G' and G'', of lysozyme and β-casein adsorption layers at the C16/water interfaces have been measured in the frequency sweep oscillatory regime. In other words, G' and G'' have been measured as functions of ω at a fixed amplitude, $\gamma_a = 2\%$. The used concentrations of lysozyme and β-casein are 5 and 8.5 mg L^{-1} (5 and 8.5 × 10^{-4} wt%), respectively; both of them correspond to 0.35 μM. pH = 7 was maintained by 100 mM phosphate buffer. The working temperature was 23 °C. The aging time of the protein adsorption layers was 24 h. During this period, equilibration and consolidation of the adsorption layer took place.

Fig. 10a shows the plots of $\langle \nu_{ch}\rangle$ *vs.* $\langle \dot{\gamma}\rangle$ for lysozyme and β-casein adsorption layers at the C16/water interface calculated from the data for G' and G'' in ref. 34. In the double-log scale, the two sets of data perfectly comply with linear dependences, and consequently, the respective viscoelastic layers obey the VT model. The values of the parameters m and Q, determined from the slope and intercept, are listed in Table 2. For comparison, the values of m and Q for β-casein layers at the air/water interface from ref. 21 are also given. The values of m for all systems in Table 2 are in the range from 0.856 to 1.04. Such values indicate that, in general, the surface elasticity and viscosity depend on $\dot{\gamma}$. We recall that the conventional Maxwell model (with constant E_{sh} and η_{sh}) corresponds to $m = 0$.

Substituting m determined from the linear plot (like that in Fig. 10a) and the experimental G' and G'' values in eqn (11) and (12), we calculate $\langle E_{sh}\rangle$ and $\langle \eta_{sh}\rangle$ *vs.* the rate of strain; see Fig. 10b. The plots show that for both lysozyme and β-casein $\langle E_{sh}\rangle$ increases, whereas $\langle \eta_{sh}\rangle$ decreases, with the rise of $\langle \dot{\gamma}\rangle$. For the lysozyme (a globular protein), $\langle E_{sh}\rangle$ and $\langle \eta_{sh}\rangle$ are markedly greater than for the disordered protein β-casein. However, for both of them the shear elasticity $\langle E_{sh}\rangle$ is considerably smaller than that for HFBII (see Fig. 9a).

In Appendix A,† it is shown that the VT model is applicable also to determine $\langle E_{sh}\rangle$ and $\langle \eta_{sh}\rangle$ from the experimental G' and G'' values measured for β-casein layers cross-linked by the enzyme transglutaminase,[35] and for asphaltene films at toluene–heptane/brine interfaces.[41] The values of the parameters m, Q and μ are determined also for these systems and compared with those in Tables 1 and 2. For both cross-linked β-casein and asphaltene $\langle E_{sh}\rangle$ and $\langle \eta_{sh}\rangle$ are considerably smaller than those for HFBII adsorption layers at the same $\langle \dot{\gamma}\rangle$; compare Fig. 9 with Fig. A1 and A2 in Appendix A.†

The comparison of the data for HFBII adsorption layers at oil/water interfaces in Fig. 9a with analogous data for other proteins

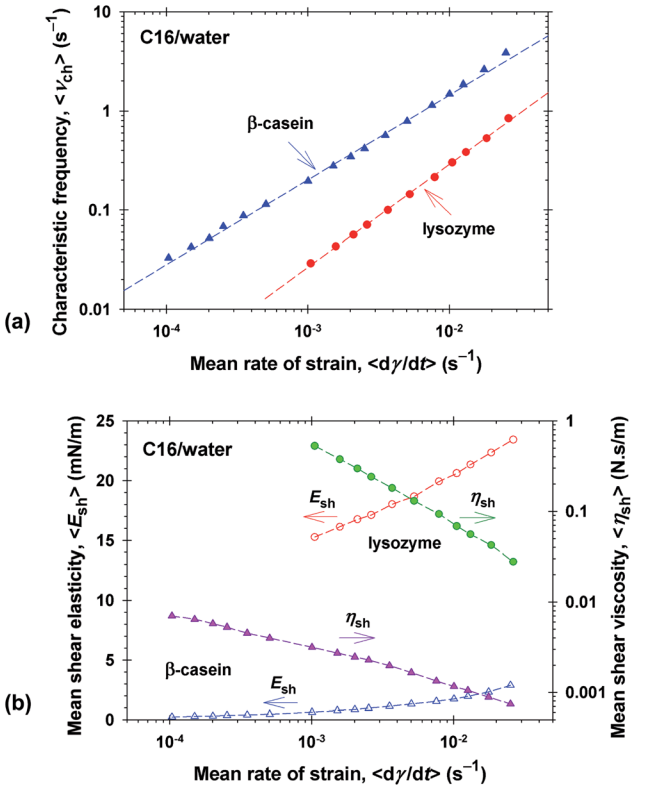

Fig. 10 Rheological parameters of lysozyme and β-casein adsorption layers at the C16/water interface determined from literature data[34] for G' and G''. (a) Plot of the characteristic frequency $\langle \nu_{ch}\rangle = G''\omega/G'$ *vs.* the rate of strain $\langle \dot{\gamma}\rangle$ in accordance with eqn (9). (b) Plots of the surface shear elasticity $\langle E_{sh}\rangle$ and viscosity $\langle \eta_{sh}\rangle$ *vs.* $\langle \dot{\gamma}\rangle$ calculated from eqn (11) and (12).

Table 2 Parameters of the VT model determined by fits of data for $\langle \nu_{ch}\rangle = G''\omega/G'$ in accordance with eqn (9)

System	m	Q (s^{m-1})	μ	Reference[a]
Lysozyme at C16/water	1.04	34	0.428	34
β-Casein at air/water	0.90	885	0.415	21
β-Casein at C16/water	0.856	74	0.411	34

[a] Source of data for G' and G''.

and amphiphiles in Fig. 10b, A1 and A2 indicate that at shear rates $\langle \dot{\gamma}\rangle = 10^{-4} - 10^{-1}$ s^{-1} the shear elasticity E_{sh} remains constant for HFBII, whereas E_{sh} increases with $\langle \dot{\gamma}\rangle$ for the other systems being considerably lower than for hydrophobin. The constancy of E_{sh} at not too high $\langle \dot{\gamma}\rangle$ seems to be a property of hydrophobin, because it is observed also with HFBII at the air/water interface; see *e.g.* Fig. 12a in ref. 21. However, for the mixed layers of HFBII with β-lactoglobulin, β-casein and Tween 20, E_{sh} exhibits a non-monotonic dependence on the shear rate: increases at the lower $\langle \dot{\gamma}\rangle$ and decreases at the higher $\langle \dot{\gamma}\rangle$.[22]

The high and constant value of E_{sh} for HFBII adsorption layers in the investigated range of shear rates could be related to the ability of the hydrophobin molecules to *strongly* and *quickly* stick to each other at the interface, which leads to the

solidification of their adsorption layer within 10 s; see *e.g.* Fig. B1 in Appendix B.† The surface solidification (the appearance of non-zero G' and E_{sh}) may take 12 h for other proteins. [24]. The shear deformation of a viscoelastic body includes breakage of cohesion contacts between neighboring molecules and establishment of such contacts with the new neighbors. In this respect, the enhanced cohesion of the HFBII molecules certainly contributes to the high surface shear elasticity of their adsorption layers.

6. Summary and conclusions

To the best of our knowledge, the present article is the first study on the surface shear rheology of hydrophobin layers at *oil/water* interfaces. Experiments in two different dynamic regimes, fixed-rate-of-strain and oscillations, have been carried out with a rotational rheometer. The rheological data obtained in both regimes comply with a viscoelastic thixotropic (VT) model, which is used to determine the surface shear elasticity and viscosity, E_{sh} and η_{sh}.

For HFBII layers, the values of E_{sh} and η_{sh} at oil/water interfaces are somewhat lower than for the air/water interface. Moreover, E_{sh} and η_{sh} depend on the nature of the oil, being smaller for the hexadecane/water in comparison with the soybean-oil/water interface. It seems that oil molecules can be incorporated in the HFBII adsorption layer, where they may reduce the hydrophobic adhesion of the protein molecules and serve as a lubricant upon shearing. In this respect, the smaller molecules of hexadecane produce a greater effect, because they can easily enter voids in the hydrophobin interfacial layer.

In addition, it is remarkable that for HFBII layers at oil/water interfaces the surface shear elasticity E_{sh} is independent of the rate of strain, $\dot{\gamma}$, in the whole investigated range of shear rates (Fig. 9a), which is not the case with HFBII at the air/water interface and with other systems (Section 5). For all investigated systems, η_{sh} decreases with $\dot{\gamma}$, *i.e.* shear thinning is observed. For oil/water interfaces, E_{sh} and η_{sh} determined for HFBII adsorption layers are considerably greater than for other proteins, like lysozyme and β-casein. It is confirmed that the hydrophobin forms the most rigid surface layer among all investigated proteins – the present data indicate that this is fulfilled not only for the air/water, but also for the oil/water interface.

Another remarkable fact is that the rheological behavior of all interfacial layers investigated here (oil/water interfaces), as well as in ref. 20–22 (air/water interfaces), comply with the VT model. In Section 5 and Appendix A,† we confirm the applicability of the VT model by analyzing literature data for adsorption layers at oil/water interfaces from lysozyme and β-casein – both native and cross-linked by an enzyme, as well as for films from asphaltene. Thus, the VT model turns out to be a versatile tool for determining the surface shear elasticity and viscosity, E_{sh} and η_{sh}, from raw data for the storage and loss moduli, G' and G''.

Acknowledgements

The authors gratefully acknowledge the support from Unilever R&D Vlaardingen; from the FP7 project Beyond-Everest, and from COST Actions CM1101, FA1001, MP1106 and MP1305. The authors are thankful to Dr Krastanka Marinova and Mr Mihail Georgiev for the interfacial tension data.

References

1 A. R. Cox, D. L. Aldred and A. B. Russel, *Food Hydrocolloids*, 2009, **23**, 366–376.
2 T. B. J. Blijdenstein, P. W. N. de Groot and S. D. Stoyanov, *Soft Matter*, 2010, **6**, 1799–1808.
3 M. Reger, T. Sekine, T. Okamoto and H. Hoffmann, *Soft Matter*, 2011, **7**, 8248–8257.
4 M. Reger, T. Sekine and H. Hoffmann, *Colloids Surf., A*, 2012, **413**, 25–32.
5 H. Hoffmann and M. Reger, *Adv. Colloid Interface Sci.*, 2014, **205**, 94–104.
6 M. Reger, T. Sekine, T. Okamoto, K. Watanabe and H. Hoffmann, *Soft Matter*, 2011, **7**, 11021–11030.
7 M. Reger and H. Hoffmann, *J. Colloid Interface Sci.*, 2012, **368**, 378–386.
8 M. Reger, T. Sekine and H. Hoffmann, *Colloid Polym. Sci.*, 2012, **290**, 631–640.
9 E. S. Basheva, P. A. Kralchevsky, N. C. Christov, K. D. Danov, S. D. Stoyanov, T. B. J. Blijdenstein, H.-J. Kim, E. G. Pelan and A. Lips, *Langmuir*, 2011, **27**, 2382–2392.
10 E. S. Basheva, P. A. Kralchevsky, K. D. Danov, S. D. Stoyanov, T. B. J. Blijdenstein, E. G. Pelan and A. Lips, *Langmuir*, 2011, **27**, 4481–4488.
11 M. Qin, L.-K. Wang, X.-Z. Feng, Y.-L. Yang, R. Wang, C. Wang, L. Yu, B. Shao and M.-Q. Qiao, *Langmuir*, 2007, **23**, 4465–4471.
12 H. Asakawa, S. Tahara, M. Nakamichi, K. Takehara, S. Ikeno, M. B. Linder and T. Haruyama, *Langmuir*, 2009, **25**, 8841–8844.
13 Z.-X. Zhao, H.-C. Wang, X. Qin, X.-S. Wang, M.-Q. Qiao, J. Anzai and Q. Chen, *Colloids Surf., B*, 2009, **71**, 102–106.
14 A. Dan, G. Gochev, J. Krägel, E. V. Aksenenko, V. B. Fainerman and R. Miller, *Curr. Opin. Colloid Interface Sci.*, 2013, **18**, 302–310.
15 D. Vollhardt and V. B. Fainerman, *Adv. Colloid Interface Sci.*, 2006, **127**, 83–97.
16 L. Liggieri, E. Santini, E. Guzmán, A. Maestro and F. Ravera, *Soft Matter*, 2011, **7**, 7699–7709.
17 E. Santini, E. Guzman, F. Ravera, M. Ferrari and L. Liggieri, *Phys. Chem. Chem. Phys.*, 2012, **14**, 607–615.
18 S. Tcholakova, Z. Mitrinova, K. Golemanov, N. D. Denkov, M. Vethamuthu and K. P. Ananthapadmanabhan, *Langmuir*, 2011, **27**, 14807–14819.
19 N. A. Alexandrov, K. G. Marinova, T. D. Gurkov, K. D. Danov, P. A. Kralchevsky, S. D. Stoyanov, T. B. J. Blijdenstein, L. N. Arnaudov, E. G. Pelan and A. Lips, *J. Colloid Interface Sci.*, 2012, **376**, 296–306.
20 G. M. Radulova, K. Golemanov, K. D. Danov, P. A. Kralchevsky, S. D. Stoyanov, L. N. Arnaudov, T. B. J. Blijdenstein, E. G. Pelan and A. Lips, *Langmuir*, 2012, **28**, 4168–4177.

21 K. D. Danov, G. M. Radulova, P. A. Kralchevsky, K. Golemanov and S. D. Stoyanov, *Faraday Discuss.*, 2012, **158**, 195–221.

22 K. D. Danov, P. A. Kralchevsky, G. M. Radulova, E. S. Basheva, S. D. Stoyanov and E. G. Pelan, *Adv. Colloid Interface Sci.*, 2014, DOI: 10.1016/j.cis.2014.04.009.

23 R. D. Stanimirova, T. D. Gurkov, P. A. Kralchevsky, K. T. Balashev, S. D. Stoyanov and E. G. Pelan, *Langmuir*, 2013, **29**, 6053–6067.

24 R. Borbás, B. S. Murray and É. Kiss, *Colloids Surf., A*, 2003, **213**, 93–103.

25 Y. Wang, C. Bouillon, A. Cox, E. Dickinson, K. Durga, B. S. Murray and R. Xu, *J. Agric. Food Chem.*, 2013, **61**, 1554–1562.

26 T. B. J. Blijdenstein, R. A. Ganzevles, P. W. N. de Groot and S. D. Stoyanov, *Colloids Surf., A*, 2013, **438**, 13–20.

27 S. O. Lumsdon, J. Green and B. Stieglitz, *Colloids Surf., B*, 2005, **44**, 172–178.

28 D. L. Cheung, *Langmuir*, 2012, **28**, 8730–8736.

29 J. Krägel, S. R. Derkatch and R. Miller, *Adv. Colloid Interface Sci.*, 2008, **144**, 38–53.

30 B. S. Murray, *Curr. Opin. Colloid Interface Sci.*, 2011, **16**, 27–35.

31 G. Doxastakis and O. Sherman, *Colloid Polym. Sci.*, 1986, **264**, 254–259.

32 L. G. Ogden and A. J. Rosenthal, *J. Colloid Interface Sci.*, 1997, **191**, 38–47.

33 E. M. Freer, K. S. Yim, G. G. Fuller and C. J. Radke, *J. Phys. Chem. B*, 2004, **108**, 3835–3844.

34 E. M. Freer, K. S. Yim, G. G. Fuller and C. J. Radke, *Langmuir*, 2004, **20**, 10159–10167.

35 R. Partanen, M. Lille and P. Forssell, *Annu. Trans. Nord. Rheol. Soc.*, 2011, **19**, 1–4.

36 S. G. Baldursdottir, M. S. Fullerton, S. H. Nielsen and L. Jorgensen, *Colloids Surf., B*, 2010, **79**, 41–46.

37 V. Ulaganathan, N. Bergenstahl, J. Krägel and R. Miller, *Colloids Surf., A*, 2012, **413**, 136–141.

38 J.-M. Jung, D. Z. Gunes and R. Mezzenga, *Langmuir*, 2010, **26**, 15366–15375.

39 N.-P. K. Humblet-Hua, E. van der Linden and L. M. C. Sagis, *Soft Matter*, 2013, **9**, 2154–2165.

40 C. Vézy, K. D. Hermanson, T. Scheibel and A. R. Bausch, *Biointerphases*, 2009, **4**, 43–46.

41 Y. Fan, S. Simon and J. Sjöblom, *Colloids Surf., A*, 2010, **366**, 120–128.

42 A. Goebel and K. Lunkenheimer, *Langmuir*, 1997, **13**, 369–372.

43 R. C. Hardy, *J. Res. Natl. Bur. Stand.*, 1958, **61**, 433–436.

44 A. G. Gaonkar and R. P. Borwankar, *J. Colloid Interface Sci.*, 1991, **146**, 525–532.

45 H. Noureddini, B. C. Teoh and L. Davis Clements, *J. Am. Oil Chem. Soc.*, 1992, **69**, 1189–1191.

46 A. R. Cox, F. Cagnol, A. B. Russell and M. J. Izzard, *Langmuir*, 2007, **23**, 7995–8002.

47 E. Aumaitre, S. Wongsuwarn, D. Rossetti, N. D. Hedges, A. R. Cox, D. Vella and P. Cicuta, *Soft Matter*, 2012, **8**, 1175–1183.

48 B. S. Murray and E. Dickinson, *Food Sci. Technol. Int.*, 1996, **2**, 131–145.

49 P. Erni, P. Fischer, E. J. Windhab, V. Kusnecov, H. Stettin and J. Läuger, *Rev. Sci. Instrum.*, 2003, **74**, 4916–4924.

50 P. Erni, P. Fischer, E. J. Windhab, V. Kusnecov, H. Stettin and J. Läuger, *Prog. Colloid Polym. Sci.*, 2004, **129**, 16–23.

51 K. Hyun, M. Wilhelm, C. O. Klein, K. S. Cho, J. G. Nam, K. H. Ahn, S. J. Lee, R. H. Ewoldt and G. H. McKinley, *Prog. Polym. Sci.*, 2011, **36**, 1697–1753.

52 D. Acierno, F. P. La Mantia, G. Marrucci and G. Titomanlio, *J. Non-Newtonian Fluid Mech.*, 1976, **1**, 125–146.

53 D. Acierno, F. P. La Mantia, G. Marrucci, G. Rizzo and G. Titomanlio, *J. Non-Newtonian Fluid Mech.*, 1976, **1**, 147–157.

54 H. A. Barnes, *J. Non-Newtonian Fluid Mech.*, 1997, **70**, 1–33.

55 I. Panaiotov, D. S. Dimitrov and L. Ter-Minassian-Saraga, *J. Colloid Interface Sci.*, 1979, **72**, 49–53.

56 P. M. Vassilev, S. Taneva, I. Panaiotov and G. Georgiev, *J. Colloid Interface Sci.*, 1981, **84**, 169–174.

57 I. Panaiotov, Tz. Ivanova, J. Proust, F. Boury, B. Denizot, K. Keough and S. Taneva, *Colloids Surf., B*, 1996, **6**, 243–260.

58 A. Hambardzumyan, V. Aguié-Béghin, I. Panaiotov and R. Douillard, *Langmuir*, 2003, **19**, 72–78.

59 Tz. Ivanova, I. Minkov, I. Panaiotov, P. Saulnier and J. E. Proust, *Colloid Polym. Sci.*, 2004, **282**, 1258–1267.

60 H. A. Barnes, *A Handbook of Elementary Rheology*; University of Wales, Institute of Non-Newtonian Fluid Mechanics, Aberystwyth, UK, 2000.